Nanoscale

REVIEW

View Article Online
View Journal | View Issue

Cite this: *Nanoscale*, 2023, **15**, 9242

Polyoxometalate-based frameworks for photocatalysis and photothermal catalysis

Xiaofei Chen, *[a] Hongzhuo Wu,[a] Xinjian Shi[a] and Lixin Wu *[b]

Received 14th March 2023,
Accepted 21st April 2023

DOI: 10.1039/d3nr01176c

rsc.li/nanoscale

Polyoxometalate-based frameworks (POM-based frameworks) are extended structures assembled from metal–oxide cluster units and organic frameworks that simultaneously possess the virtues of POMs and frameworks. They have been attracting immense attention because of their diverse architectures and charming topologies and also due to their probable application prospects in the areas of catalysis, separation, and energy storage. In this review, the recent progress in POM-based frameworks including POM-based metal organic frameworks (PMOFs), POM-based covalent organic frameworks (PCOFs), and POM-based supramolecular frameworks (PSFs) is systematically summarized. The design and construction of a POM-based framework and its application in photocatalysis and photothermal catalysis are introduced, respectively. Finally, our brief outlooks on the current challenges and future development of POM-based frameworks for photocatalysis and photothermal catalysis are provided.

1 Introduction

Polyoxometalates (POMs), which are comprised mainly of early-transition metal ions (*e.g.*, W, Mo, V, Nb, Ta) in their highest oxidation states (+4, +5, +6) through oxygen bridges, have evolved into a type of molecular nanocluster with a well-defined composition and uniform architecture showing a wide range of applications in nanoscience, energy catalysis, medicine, biology, and other fields.[1–4] POMs can be considered

[a]*Key Laboratory for Special Functional Materials of Ministry of Education, National & Local Joint Engineering Research Center for High-Efficiency Display and Lighting Technology, Henan University, Kaifeng 475004, China.*
E-mail: chenxf22@henu.edu.cn
[b]*State Key Laboratory of Supramolecular Structure and Materials, College of Chemistry, Jilin University, Changchun 130012, China.*
E-mail: wulx@jlu.edu.cn

Xiaofei Chen

Xiaofei Chen received her Ph.D. degree in polymer chemistry and physics from Jilin University under the supervision of Prof. Lixin Wu in 2021. Currently, she works at the Key Laboratory for Special Functional Materials of the Ministry of Education, Henan University, China. Her current research focuses on the synthesis and self-assembly functionalization of polyoxometalate complexes.

Lixin Wu

Lixin Wu received his Ph.D. degree in chemistry from Jilin University in 1993. He then joined the Institute of Theoretical Chemistry as a faculty at Jilin University and became a postdoctoral researcher at Changchun Institute of Physics, Chinese Academy of Sciences and later went to Hokkaido University as a senior JSPS fellow. After about two years of research at the University of Hong Kong, he was promoted to a full professor in 2000. His research involved inorganic polyoxometalate chemistry, colloid and interface chemistry, and supramolecular self-assembly. Now, his group focuses on POM-based porous materials, biomaterials, and near-infrared photothermal catalysis.

analogs of semiconducting metal oxides, as they both consist of d^0 transition metals and exhibit similar electronic properties, including a well-defined highest occupied molecular orbital (HOMO)–lowest unoccupied molecular orbital (LUMO) gap.[5–8] Owing to their intriguing properties, including impressive sensitivity to UV light, tunable redox properties, and high thermal stability, POMs are promising candidates for use in heterogeneous photocatalysis. The fast photo-responsive charge transfer and reversible multiple electron and proton redox reactions play a very important role in promoting the photocatalytic performance.[9,10] However, POMs exhibit weak absorption in the visible spectrum and a longer wavelength, and its photoexcitation usually requires irradiation with UV light;[11–13] thus, the utilization efficiency of solar energy is usually low. In addition, their application is largely restricted by factors such as a small specific surface area (less than 10 m^2 g^{-1}), easy self-aggregation, and low stability in an aqueous solution.[14,15] Structural dispersion and stability are the prerequisites for POM chemistry to be applied in heterogeneous catalysis. POMs as superior inorganic building blocks are often used to assemble a well-defined architecture.[16–18] Abundant surface oxygens of POMs endow them with active sites to coordinate with metal ions and build up high-dimensional coordinated complexes;[19,20] moreover, discrete anions make them a good non-covalent binding site.[18,21] The framework chemistry, especially involving the most attractive structures of metal–organic frameworks (MOFs),[22] covalent organic frameworks (COFs),[23] and supramolecular frameworks (SFs),[24] has been greatly advanced due to its controllable synthesis, tunable structure, and potential applications. Generally, framework structures contain photoactive building blocks such as porphyrin, aniline, viologen, π systems and so on, which can broaden the spectral range to the visible light region, and their porosity and large specific surface area make them excellent photocatalysts.[25,26] In addition, nanoparticles can also be loaded for photocatalysis. These well-defined architectures and POMs each have their own advantages, and integrating them unambiguously results in novel structures that derive properties directly from POMs or synergizes between POM units and frameworks.[27] For example, the adjustable light absorption of MOFs endows POMs with the catalytic ability in the full-spectrum region; substrates can only access the surface sites of non-porous POM catalysts, however for porous POM structures, internal catalytic centers can be easily accessed in confined spaces, endowing them with special catalytic properties. Clear evidence of the attention gathered by photocatalysis is the huge number of scientific articles published every year on this topic. Therefore, seeking a new, efficient, and cheap photocatalyst is still a hot topic in this area. In addition, photothermal catalysis over POMs is at a nascent stage but exhibits significant promoting effects toward heterogeneous organic reactions.

In this review, the development of various classic POM-based frameworks mainly including POM-based metal organic frameworks (PMOFs), POM-based covalent organic frameworks (PCOFs), and POM-based supramolecular frameworks, (PSFs), and their application in photocatalysis and photothermal catalysis in the past five years are outlined. Finally, our perspectives on current challenges and future development of POM-based frameworks for photocatalysis and photothermal catalysis are briefly discussed.

2 Design strategies of POM-based frameworks

Recently, numerous POM-based frameworks have been designed and synthesized ranging from single clusters, POM-based assemblies, POM-based organic–inorganic hybrids, *etc*.[9] Considering that the absorption range of POMs is relatively narrow, as a kind of excellent inorganic building block, the organic modification of POMs is one of the most important research topics in POM chemistry because it can tune the physicochemical properties of POMs. Therefore, in this section, we mainly introduce organic–inorganic hybrid POM-based frameworks, which is mainly classified from the interaction, PMOFs, PCOFs and PSFs.

2.1 PMOFs

Framework structures, an emerging class of highly porous materials that consist of organic ligands and inorganic metal clusters or ions, have been extensively studied in past decades, such as MOFs and COFs.[28,29] Owing to the unique structural features of permanent porosity, high surface area, tunable pore size/shape, and uniform open cavities, frame structures have received special attention in the fields of gas storage, separation, and catalysis.[30] Both organic linkers and metal nodes in the framework structure can play important roles in photocatalytic reactions. The organic linkers can be tuned to act as light-harvesting units, and metal clusters/ions can be viewed as isolated semiconducting sites, which can be activated by organic linkers or excited upon light irradiation to achieve photo-responsiveness at long wavelengths. In addition, due to the diversity of organic linkers and metal clusters/ions, as well as the diverse assembly, the light absorption properties of framework structures can be rationally designed and tailored through the selection of organic linkers and metal clusters or ions. In addition, the framework structure with an ultra-high porosity, a large surface area, and open channels makes abundant catalytic sites accessible and also greatly facilitates substrate/product transport/diffusion, thus becoming the most promising conventional photocatalyst. In both cases, it is seen that the combination of POMs with MOFs or COFs yields additional properties in the enhanced catalysis and selectivity of products.

PMOFs are mainly based on coordination bond-driven synthesis from nitrogen and oxygen-donor ligands used as organic linkers to connect with POMs *via* coordination bonds.[31–33] The high negative charge and abundant oxygen atoms on the surface of POMs can coordinate with cationic metal centers and/or organic ligands directly.[34–36] Different types of POMs, including Anderson, Keggin, and Dawson

POMs, have been explored.[37] When POMs serve as building units of MOFs, the saturated POMs and transition metal-substituted POMs are generally selected to coordinate with the metal ions or cluster.[38] For example, Liu *et al.* used Keggin POMs to induce Ni^{2+} to coordinate with BPY ligands, thereby forming an open POM-based framework.[39] POMs have also been used as ideal secondary building units to construct PMOFs through covalent interactions. Lan *et al.* reported a stable 3D open framework. linking zinc-terminated ε-Keggin POMs with organic ligands.[40] These two methods are often synthesized using metal ions, organic ligands and POM precursors *via* conventional hydrothermal or solvothermal methods. POMs are directly connected with organic ligands or bounded with metal centers and organic linkers. That is, POMs are part of the frameworks of PMOFs. Considering that a variety of studies have been developed and applied to various fields, and some reviews have already summarized the synthesis and application of these materials.[41] Here, we will focus on the examples constructed by the following methods.

Aside from serving as building units, POMs are also applied as guest components to be incorporated into the MOF cavities with molecular dispersion (Fig. 1a).[42] The key difference in the latter is that POMs are not part of frameworks and are embedded within the pore architecture of MOFs (MOFs and POMs can be described as the host and guest). The synthesis is mainly classified into two categories: impregnation and encapsulation.[36] The impregnation method involves soaking the preformed MOFs in a suitable POM solution so that a match of the pore size and POM diameter is required to allow uptake. If these conditions are met, the method is applicable and can be performed under mild conditions, making it suitable even for thermally and chemically sensitive POMs. However, the drawbacks are also obvious, namely, low maximum loading, low uniformity, large cavity occupation, and possible leaching under operating conditions, especially for POMs located at or near the surface of MOF particles. In contrast, encapsulation can be used when the POM diameter is greater than those of the MOFs. Here, the MOFs assemble around the preformed POMs, usually under solvothermal conditions, and the solid product may crystallize into a new single-crystal material in which the POMs are irreversibly "trapped" in the MOF pores. To ensure the successful synthesis, the POMs should be stable during the synthesis of PMOFs. Thus, this approach can minimize the leaching and aggregation of encapsulated POMs and can even be used to stabilize structurally unstable POM species. However, the confined pore environment also leads to pore blockage, slowed diffusion, and thus reduced reactivity.

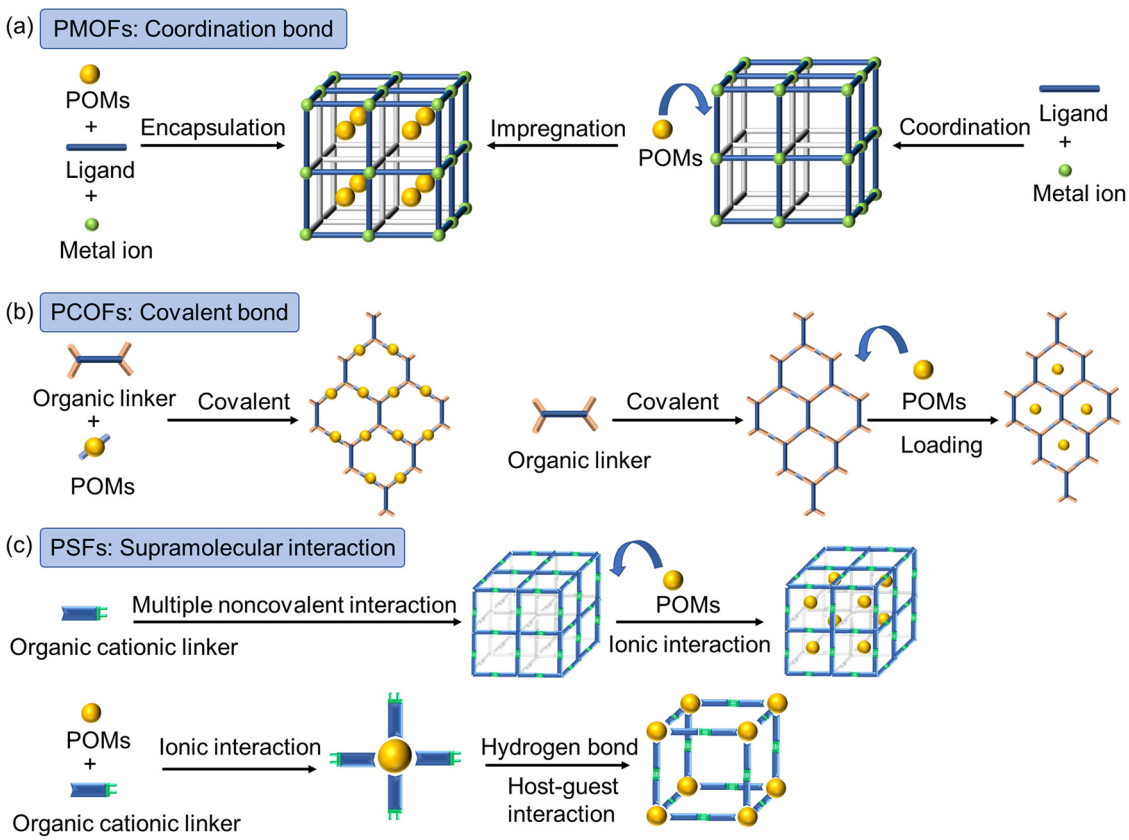

Fig. 1 Synthesis strategies and interactions for constructing (a) POM-based metal–organic frameworks (PMOFs); (b) POM-based covalent-organic frameworks (PCOFs); and (c) POM-based supramolecular frameworks (PSFs). Frames of MOFs: black and grey sticks; COFs: blue and orange sticks; organic linkers in SFs: green-blue bicolored sticks; metal ions: green spheres; POMs: dark yellow spheres.

2.2 PCOFs

POM-based frameworks can not only be synthesized in the construction of coordination architectures *via* metal–ligand interactions between POMs and organic ligands, but also be built from the covalent linkage of POM hybrid and organic building blocks (PCOFs) (Fig. 1b). COFs are two-dimensional (2D) and three-dimensional (3D) organic frameworks with large structures, which are made entirely of light elements (H, B, C, N and O) through strong covalent bonds. The PCOF reports are very rare. Tris(hydroxymethyl)methane-R (R-tris) is a commonly used group to modify POMs, achieved by the replacement of surface oxygen atoms with the hydroxyl groups of tris. When the R group is a coordinating unit, such as pyridyl or carboxylate groups, the R-tris-functionalized POMs are regarded as metalloligands.[43,44] When NH_2-tris is used, the hybrid POMs can be used as organic linkers to construct PCOFs.[45] All the archetypal Anderson, Lindqvist, and Dawson clusters can be functionalized with tris.[15,46–50] Recently, O. M. Yaghi's group reported a 3D PCOF with a 3-fold interpenetrated diamond topology *via* the imine condensation of an (amino-tris)-functionalized [$MnMo_6$]-POM linker and 4-connected tetrakis(4-formylphenyl)methane.[51] When the counter cation TBA^+ was exchanged as Li^+, this hybrid framework became a prime candidate for solid-state electrolytes with high ionic conductivity, high Li^+ transference number, and good interfacial properties. Following the same method, Yang *et al.* changed the organic linkers to 4-connected tetrahedral tetrakis(4-formylphenyl)silicon (TFPS) building units to obtain a new porous backbone M-Anderson-COF.[52] Fang *et al.* also constructed two 3D PCOFs (JUC-525 and JUC-526) featuring a 3-fold interpenetrated ***dia*** topology from NH_2-$MnMo_6$-NH_2, TFPM, and TFPS with strong covalent bonds. The POM functionalized framework showed a high reversible capacity (>550 mA h g^{-1}), rate capacity, and cycling performance (>500 cycles).[53] Zhang *et al.* chose an Anderson-type POM containing two active amino groups, NH_2-$CoMo_6$, as the building block and used the imine bond as the linkage generated by a covalent linkage of the aldehyde group, resulting in a 2D staggered stacking layered structure with an ***sql*** topology.[54] Furthermore, some post-synthetic modification strategies have also been reported to construct PCOF architectures. Generally speaking, this method is usually used to first synthesize the COF structure and immobilize POMs with covalent or non-covalent interactions.[55,56] Yan and Peng *et al.* incorporated POMs into the prepared cation COFs with electrostatic interactions.[57,58] To date, PCOFs still remain largely unexplored due to the difficult organic grafting of POMs and the low chemical tolerance of POM hybrids.

PMOFs and PCOFs have made more progress and showed excellent functionality, while some inherent weaknesses of PMOFs or PCOFs, such as structural stability and processibility in solutions, should be improved greatly, which is not conducive to displaying more functional devices.

2.3 PSFs

Compared with the rigid structures of MOFs and COFs, supramolecular frameworks (SFs) based on noncovalent interactions have attracted extensive attention due to their flexibility, dynamic tunability, and unique solution processability.[59,60] In addition to PMOFs and PCOFs, PSFs driven by noncovalent interactions have also been reported (Fig. 1c).[61] Among many noncovalent interactions, electrostatic interactions, which have relatively flexible directionality between building blocks, are widely used.[62] In general, although ionic interactions can lead to satisfactory structural strength, assembled structures with a long-range order are still rarely reported and often need to be fine-tuned according to the expected functional properties. In addition, the tunability of non-covalent interactions also brings dynamic properties to the framework that are quite different from those in coordination and covalent frameworks, extending their functionality.

POMs also provide the possibility to be incorporated into the cavities in SFs, which is the same as those used in MOFs and COFs *via* electrostatic interaction instead of coordination and covalent bonding.[63] As a typical example, Li *et al.* reported that Dawson POMs $[P_2W_{18}O_{62}]^{6-}$ have been introduced into the hollow cavity of the SF formed from the host–guest interaction of cucurbit[8]uril and a hexa-armed $[Ru(bpy)_3]^{2+}$-based precursor.[64] As for the other case, POMs as building blocks participate in the formation of SFs. Specifically, to obtain a flexible ionic framework based on electrostatic interaction, POMs with multiple negative charges and functional organic components with positive charges are combined by electrostatic interaction to obtain a reverse-micelle-like organic–inorganic hybrid serving as building blocks. Then, how to connect the building blocks is the critical issue to construct SFs, which puts high design requirements on the terminal structure of the organic moiety. As we know, the non-directionality of electrostatic interaction and the delocalization of surface charges on POMs are not conducive to the formation of regular periodic structures. Therefore, the common method is mainly to introduce new binding sites for covalent/noncovalent modification into the terminal of organic cations. Wu *et al.* constructed SFs by coating POMs with bolaform cations, which showed that increasing the cation head can effectively utilize the steric hindrance effect to realize the orderly assembly of cations around POM clusters, thereby forming SFs.[65] Compared to electrostatic interaction, it may be a good solution to modify the hydrogen bond site in the terminal of the organic part. The introduction of single or multiple hydrogen bonds, such as guanines, polyurea,[66] and ureidopyrimidinone,[67] can form 1D, 2D and 3D assembly framework structures.[68] The host–guest interaction is also an important driving force for constructing SFs.[69] By covalently modifying host or guest molecules, and then regulating the host–guest interaction between them, various PSF structures can be obtained. For example, electrostatic interactions are exploited to combine a monocation pillar[5]arene and a polyanion $[SiW_{12}O_{40}]^{4-}$ for preparing an organic–inorganic ion complex

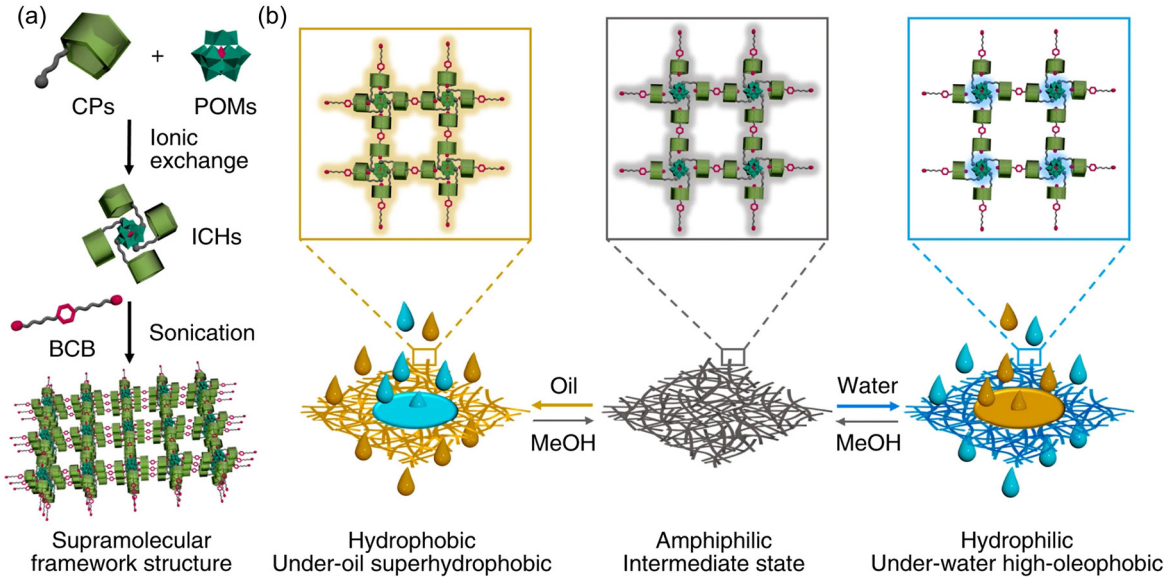

Fig. 2 (a) Schematic formation of a supramolecular framework driven by pre-ionic and post host–guest interactions, where CPs denote cationic pillar[5]arenes and ICHs mean the ionic complex hosts. (b) Modulation of membranes *via* an intermediate state (gray) for changing over in oil (yellow) and water (blue) separation. Reproduced from ref. 70. Copyright 2022, Springer Nature.

host unit. A [4 + 2] type 2D SF has been successfully prepared by utilizing the host–guest interaction between methyl pillar[5]arene and the cyano group (Fig. 2a).[70] Furthermore, under continuous ultrasonic stimulation, the interface energy drives the optimization of the internal conformation of the supramolecular polymer to form a supramolecular framework gel. Using spin-coating or drop-coating, supramolecular scaffold gel films can be fabricated on arbitrary substrates, and the amphiphilic SF becomes hydrophobic after being permeated by oil, allowing oil to pass through while water is blocked. If the amphiphilic SF is permeable to water, water can pass through the SF while oil is blocked. An interesting feature is that, methanol as a "joystick" solvent, both hydrophobic and hydrophilic SFs can be tuned to be amphiphilic, enabling *in situ* continuous switchable liquid/liquid separation (Fig. 2b).

The synergistic effect between POMs and frameworks can produce excellent properties. A POM-based framework, as a promising nano platform, has been widely investigated by researchers in recent years for its application in various fields. Although there have been some comprehensive reviews outlining its development history and applications. In this paper, we mainly review the representative applications of POM-based frameworks in photocatalysis and photothermal catalysis in recent five years. Moreover, this paper may provide an up-to-date reference for scientific researchers involved in this field.

3 Currently developed POM-based frameworks for photocatalysis

Photocatalysis, as one of the most promising ways to efficiently utilize solar energy, has been widely investigated in many research fields, such as the CO_2RR, water splitting, selective oxidation of organics, *etc*. Generally speaking, a good photocatalyst often needs to possess several factors: wide-spectrum absorption capability, high separation efficiency of holes and electrons, and high catalytic activity and selectivity. POM-based frameworks integrate the dual advantages of POMs and frameworks, showing a unique advantage in photocatalysis. For example, (1) the structural tunability of frameworks provides a great opportunity to extend the light response over a broad range; (2) the quasi-semiconductor nature of POMs and the electron transfer between MOFs and POMs can help in electron–hole (e^-–h^+) separation; (3) the high porosity and organic part of frameworks can be tailored to satisfy different POMs and catalytic reactions; (4) frameworks as heterogeneous supports favor the recycle and reuse. Because of these merits, great efforts have been devoted to developing POM-based framework materials toward photocatalysis in recent years.

3.1 Photocatalytic CO_2 reduction

Photocatalytic CO_2 reduction to green solar fuels provides a solution to growing energy demand and current global warming, which involved the following three main steps: (i) absorption of light photons with larger energy than its forbidden band gap by the photocatalyst and lead to the generation of e^-–h^+ pairs, (ii) separation and migration of the photoexcited e^-–h^+ pairs to the surface of the photocatalyst, and (iii) photoexcited e^- with the sufficient reduction potential can reduce CO_2 into CO or hydrocarbons, such as HCOOH, HCHO, CH_3OH, and CH_4; meanwhile, the generated h^+ can oxidize water to produce O_2.[71]

In 2022, Dranznieks *et al.* unveiled the reason why the immobilization of polyoxometalates (POMs) near the catalytic

center of metal–organic frameworks (MOFs) contributes to boosting the photocatalytic activity. (PW_{12}, RhCp*)@UiO-67 as was used a model catalyst to investigate its photocatalytic activity for CO_2RR and HER in acetonitrile with $[Ru(bpy)_3]^{2+}$ as the photosensitizer (PS) and triethanolamine (TEOA) as a sacrificial electron donor by combining theoretical density functional theory and microscopic kinetic modeling approaches with experimental photophysics and spectroscopic techniques.[72] The results show that PW_{12} encapsulated in MOFs acts as an electron reservoir, accepting an electron from the photogenerated reduced form $[Ru(bpy)_3]^{+}$ and transferring the electron to the catalytic site Rh (Fig. 3a). In the process, by means of microkinetic models, the comparison of POM-free and POM-containing catalysts reveals that storing electrons in POMs benefits the overall catalytic activity by favoring the reduced $[Ru(bpy)_3]^{+}$ back to the oxidate and over the unproductive degradation. This boosts the CO_2RR and HER activity by allowing the PS to involve in several catalytic cycles before decomposing. Furthermore, the computational exploration is extended to the other POMs aiming to establish the relationships between the redox potential and the activity of the related POM-containing catalysts. This clarifies that both the ability of the POMs to accept electrons and that of its reduced form to reduce the Rh catalyst are maximized, leading to a volcano plot whereby POMs with a moderate redox potential display the highest impact on photocatalytic performances (Fig. 3b).

In 2018, Liu *et al.* reported an efficient photocatalyst named Au@NENU-10 for highly efficient CO_2 reduction. For this photocatalyst, $[PTi_2W_{10}O_{40}]^{7-}$ (PTiW)-encapsulated into HKUST-1 is denoted as NENU-10 and Au NP-loaded NENU-10 as Au@NENU-10.[73] In Au@NENU-10, Au NPs mainly harvest visible light and HKUST-1 can concentrate on CO_2 molecules, and PTiW acts as a reservoir for electrons and protons, more importantly, as an active site to promote CO_2 reduction. As a control, Au@NENU-3 was also fabricated by substituting PTiW for PW_{12}, while Au@NENU-10 shows higher CO_2 reduction activity and selectivity under λ > 420 nm visible light irradiation, about 85.3-fold and 5.2-fold enhancement, respectively, corresponding to the CO_2-to-CO and CO_2-to-H_2 conversion in contrast to Au@NENU-3, which is due to the stronger protonation of Ti=O and Ti–O–W.

Covalent organic frameworks (COFs) as novel visible-light responsive photo-catalysts confront the problem of low photocatalytic activity due to the difficulty in the separation of photogenerated charge carriers. Herein, the fabrication of nano COF/POM composites to enhance the charge separation efficiency *via* cascade electron relay is reported. Lan *et al.* proposes a versatile strategy to uniformly disperse POMs into COFs by covalent linkage to confine POM clusters within the regular nanopores of COFs for the first time (Fig. 4a).[74] The COF–POM complex showed excellent light absorption, electron transfer, and suitable catalytically active sites. Therefore, they exhibit excellent catalytic activity in the CO_2 photoreduction reaction with H_2O as the electron donor (Fig. 4b). Among them, TCOF-$MnMo_6$ achieved the highest CO yield (37.25 μmol g^{-1} h^{-1} with *ca.* 100% selectivity) in a gas–solid reaction system. Furthermore, mechanistic studies based on DFT calculations revealed that the photoinduced electron transfer PET process occurred from COFs to POMs, followed by CO_2 reduction and H_2O oxidation on POMs and COFs, respectively. This work developed a method to uniformly disperse POM clusters into COFs, which also shows the potential of using COF–POM functional materials in the field of photocatalysis.

3.2 Photocatalytic water splitting

Photocatalytic splitting of water to produce hydrogen and oxygen is an effective approach to deal with the energy crisis in green and energy chemistry.[75] Water splitting generally involves two half-reactions: the HER and OER. In the overall process, three photocatalytic steps are involved, the first two steps involve the generation, separation, and migration of e^-–h^+ pairs, which are the same as those in the photocatalytic CO_2RR. The third step refers to the reduction of H^+ to H_2 by e^- (HER) and the oxidization of H_2O to O_2 by h^+ (OER).[37] To achieve photocatalytic water splitting, the top level of the VB of

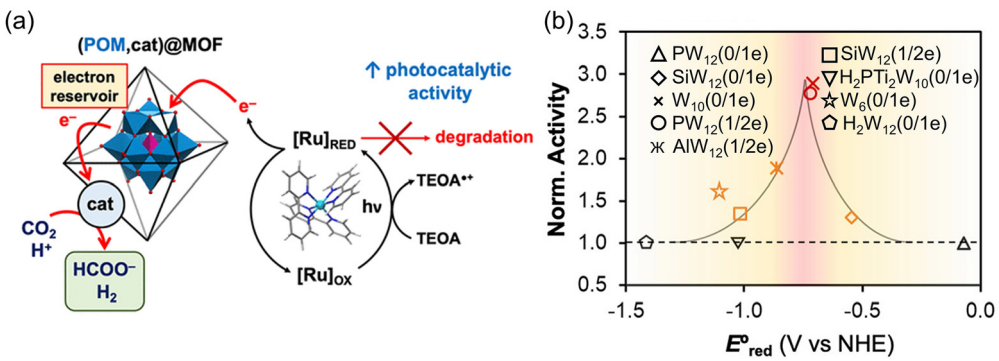

Fig. 3 (a) Schematic representation of the key steps involved in the photocatalytic reduction of CO_2 and H^+ by the POM-containing (PW_{12}, RhCp*)@UiO-67 catalyst. (b) Volcano plot of the catalytic activity of (POM, RhCp*)@UiO-67 catalysts normalized by that of the RhCp*@UiO-67 system *vs.* the redox potential of the encapsulated POM. The gray lines are depicted to guide the eye. Reproduced with permission from ref. 72. Copyright 2022, American Chemical Society.

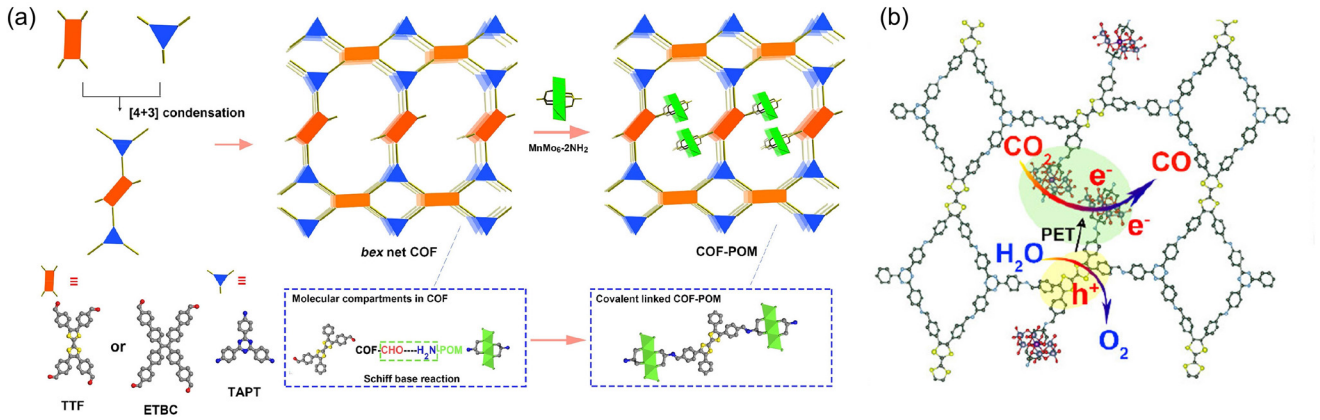

Fig. 4 (a) Schematic representation of uniformly dispersed POM clusters in COFs by confining them into the pores of COFs through covalent linkages. (b) Schematic of the mechanism of TCOF-$MnMo_6$ for the CO_2RR coupled with H_2O oxidation. Reproduced with permission from ref. 74. Copyright 2022, American Chemical Society.

the photocatalyst must be more positive than the redox potential of O_2/H_2O (1.23 V *vs.* NHE, pH = 0), while the bottom level of the CB must be more negative than the redox potential of H^+/H_2 (0 V *vs.* NHE, pH = 0). Therefore, the band gap energy (E_g) of photocatalysts for water splitting should be greater than 1.23 eV.[76] Notably, only semiconductors with a relatively narrow bandgap (E_g < 3 eV) are suitable for photocatalytic water splitting.[77] It is well known that e^-–h^+ generated by photoexcitation is easily recombined, leading to a significant decrease in the water splitting efficiency.[78] In the HER, the electron donors (sacrificial agents) are often used to consume the h^+ on the surface of photocatalysts in order to reduce the e^-–h^+ recombination, such as triethanolamine (TEOA), lactic acid, ascorbic acid, ethanol, and methanol.[79] On the other hand, oxidizing reagents (electron scavengers such as DMPO, Fe^{3+}, and Ag^+) are widely used to consume photogenerated electrons in the OER.

In 2018, Dolbecq A. *et al.* immobilized a sandwich POM $[(PW_9O_{34})_2Co_4(H_2O)_2]^{10-}$ ($P_2W_{18}Co_4$) in porphyrinic MOF-545's hexagonal channels by a mild aqueous impregnation progress for water photo-oxidation (Fig. 5a–d).[80] Simulated annealing-DFT calculations suggest that the POM is hosted between two Zr_6 clusters while surrounded by two adjacent porphyrins, in a position consistent with its oxidation by the oxidized porphyrinic linkers required upon photocatalysis. DFT calculations indicate that a particularly dense network of host–guest hydrogen bonds stabilizes $P_2W_{18}Co_4$, whereby the Co-OH_2 catalytic site is exposed to a hydrophilic environment at the PMOF interface, which may provide ideal shuttling of protons and water molecules from the solvent. The synergistic catalysis over $P_2W_{18}Co_4$@MOF-545 has proposed in Fig. 5e. The reaction mechanisms imply the following steps: (1) light capture by the porphyrin; (2) one-electron oxidation of the excited state by the sacrificial electron acceptor; (3) one-electron oxidation of the

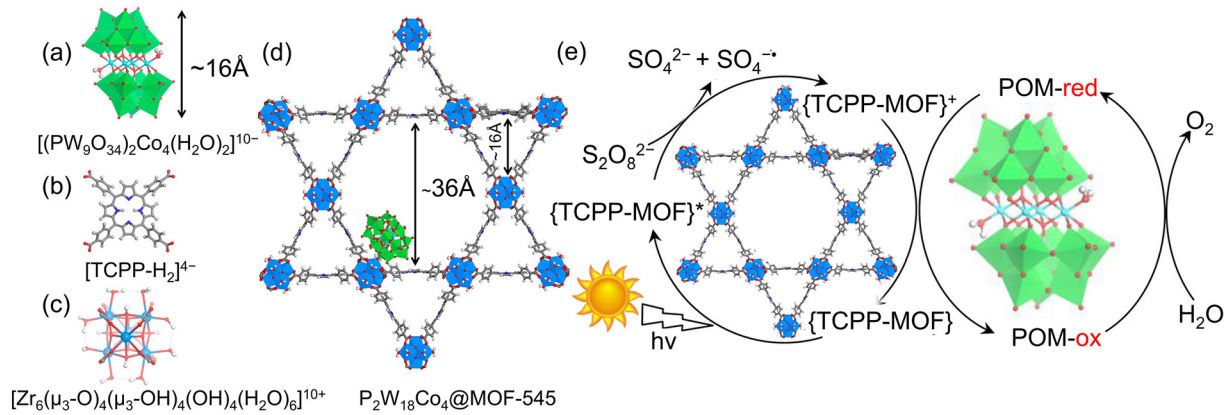

Fig. 5 POM@MOF-545 components: (a) $P_2W_{18}Co_4$ POM; (b) TCPP-H_2 linker; (c) Zr-based unit; and (d) $P_2W_{18}Co_4$@MOF-545. The position of the POM is obtained from computations. WO_6, green polyhedra; ZrO_8, blue polyhedra or spheres; Co, cyan spheres; O, red spheres; C and H, gray; N, dark blue. (e) Schematic representation of the proposed mechanism for the light-driven OER by $P_2W_{18}Co_4$@MOF-545. Adapted with permission from ref. 80. Copyright 2018, American Chemical Society.

POMs; and (4) after accumulation of 4 oxidizing equivalents on the POMs, oxidation of water into O_2. Based on this work, the same researcher group developed an easy-to-use and recyclable $P_2W_{18}Co_4$@MOF-545 thin film for photocatalytic O_2 evolution in 2019.[81] In contrast to $P_2W_{18}Co_4$@MOF-545, the TONs of $P_2W_{18}Co_4$@MOF-545-EP and $P_2W_{18}Co_4$@MOF-545-DC reached up to ~7-fold and ~25-fold enhancements, respectively.

In another report, Lv *et al.* reported two POM-based MOF composites, Ni_3PW_{10}@NU-1000 and $Ni_3P_2W_{16}$@NU-1000, through the strong host–guest interaction using a facile and broad-spectrum impregnation method (Fig. 6).[82] Under minimally optimized conditions, the two catalysts can effectively photocatalytic generation of hydrogen from a water-compatible and no noble-metal system, achieving the H_2 evolving rate of 3482 and 13 051 μmol g^{-1} h^{-1} for Ni_3PW_{10}@NU-1000 and $Ni_3P_2W_{16}$@NU-1000, respectively. The experiment results show that higher catalytic activity is stemming from the electron-deficient $[P_2W_{15}O_{56}]$ ligand in $Ni_3P_2W_{16}$ can obviously store more electrons than that of the $[PW_9O_{34}]$ ligand in Ni_3PW_{10}, and $Ni_3P_2W_{16}$ exhibits a more suitable size in the NU-1000 host, avoiding leaching. Furthermore, the photocatalytic mechanism indicates that the photoexcited state [TBAPy-Zr(IV)]* could transfer the electron to the $Ni_3P_2W_{16}$ catalyst site to promote the HER process.

3.3 Photocatalytic selective oxidation of organics

POM-based frameworks are also used as efficient photocatalysts for the selective conversion of organics to high-added chemicals, for example, oxidation of sulfides, alcohol, alkene, and C–H in aromatics.[83] Niu *et al.* prepared {[Zn(HPYI)$_3$]$_2$(DPNDI)}[$BW_{12}O_{40}$]$_2$ (ZnW-DPNDI-PYI) and used in the photocatalytic coupling of primary amines and olefins epoxidation with O_2 under visible-light conditions (Fig. 7a).[84] Later, a novel PMOF photocatalyst, Co_4W_{22}-DPNDI, was designed and prepared by incorporating the unusual sandwiched-POM Co_4W_{22} into the photoactive organic bridging link DPNDI framework using a hydrothermal method.[85] The directional arrangement of photosensitizers DPNDI and POMs in a confined space facilitates electron–hole separation and creates a short migration path for charge carriers that ensures electron transfer and proton migration. Co_4W_{22}-DPNDI exhibits high catalytic activity for the activation of the C(sp^3)–H bond of toluene using light as a driving force and H_2O as an oxygen source under mild conditions. This study provides a powerful approach to designing novel photocatalysts and a green and economical way to functionalize inert C(sp^3)–H bonds. Following a similar method, a Zn-substituted Keggin polyanion $[SiZnW_{11}O_{39}]^{6-}$ is incorporated into a photoactive 2,4,6-tri(4-pyridyl)-1,3,5-triazine (TPT) framework (Fig. 7b). The direct coordination bond between $[SiZnW_{11}O_{39}]^{6-}$ and the TPT ligand and the π–π interactions between TPT molecules help to separate and migrate photogenerated carriers, which improves the photocatalytic activity of hydrazine hydrate with 99% conversion and selectivity for anilines under mild conditions.[86] Very recently, Wang and Niu *et al.* constructed two crystalline PMOFs (CoW-1 and CoW-2) through assembling $Co^{II}W_{12}$ chromophores into Cu-BPY MOFs, whose light absorptions extend to the visible region due to MMCT effects.[87] The Cu–O–W covalent bonds constructed in CoW-1 promote the carrier separation efficiency, thus achieving higher activity (AQY = 17.5% at 595 nm) in the coupling reaction of benzyl alcohol with aniline under >420 nm visible light irradiation.

Not only that, POM-based frameworks also exhibit outstanding heterogeneous photocatalytic activities toward degrading organic dyes in water.[88] The mechanism involved is mainly organic pollutants (*e.g.*, antibiotics, dyes, *etc.*) can be degraded by $^{\bullet}OH$ and $O2^{\bullet-}$ generated on the VB and CB of the catalyst, respectively. In addition, the pollutants can also be directly degraded by photoexcited h^+.[89] Yang *et al.* constructed three iso-structural Anderson PCOFs, M-Anderson-COFs (M = Mn, Co, Fe), through imine condensation (Fig. 7c), in which Mn-Anderson-COFs exhibited excellent photocatalytic performance for the degradation of RhB and MB in water. The addition of different scavengers demonstrated that $^1O_2$ and H_2O_2 were primary reactive species to degrade the dyes.[52] Very

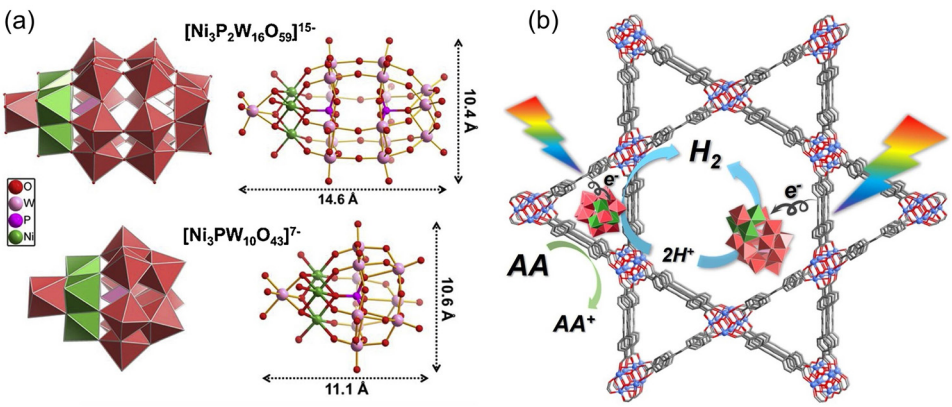

Fig. 6 (a) Ball-and-stick and polyhedral crystal structures and sizes of two different tri-Ni-substituted POMs. (b) Proposed mechanism for the HER over $Ni_3P_2W_{16}$@NU-1000. Adapted with permission from ref. 82. Copyright 2021, Elsevier.

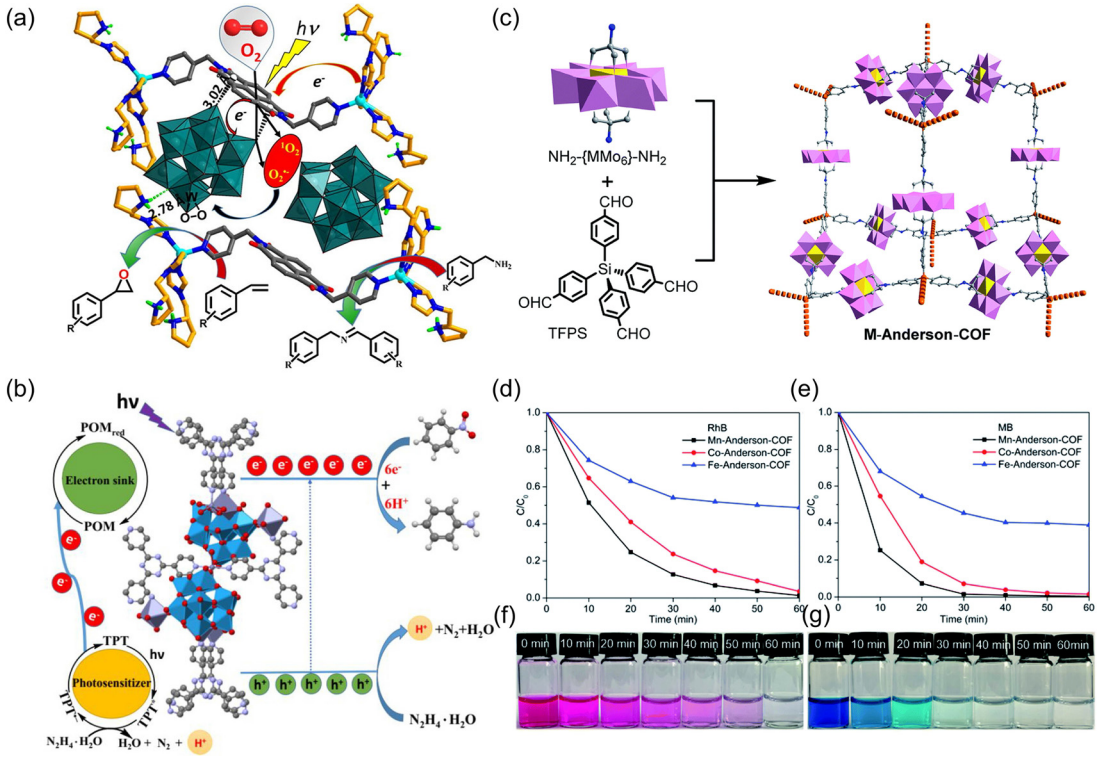

Fig. 7 (a) The design concept for obtaining photocatalysts and the representation of selective benzylamine and olefin oxidation over ZnW-DPNDI-PYI by photocatalysis. Adapted with permission from ref. 84. Copyright 2019, Elsevier. (b) Design concept of the {ZnW-TPT} photocatalyst for the reduction of nitroarenes. Adapted with permission from ref. 86. Copyright 2022, American Chemical Society. (c) Synthetic strategy and structural illustration of M-Anderson-COFs. Photodegradation of (d) RhB and (e) MB using a M-Anderson-COF catalyst (0.1 mg mL^{-1}) in water. *C* is the dye concentration after a certain period of light irradiation and C_0 is the dye concentration (100 mg L^{-1}) after reaching the adsorption/desorption equilibrium in the dark. The color change of (f) RhB and (g) MB was observed using an Mn-Anderson-COF as the catalyst. Adapted with permission from ref. 52. Copyright 2020, Royal Society of Chemistry.

recently, as viologen is a type of excellent photoactive ligand, a $[\theta\text{-}Mo_8O_{26}]^{4-}$-based cobalt–viologen 2D framework (BHU-1) was constructed and used as a multifunctional photocatalyst for CEES oxidation, Cr(VI) reduction, and RhB decolorization under different light regimes. Under full spectrum/visible/NIR light irradiation, the conversion and selectivity of CEES were 99%/96%, 98%/97%, and 93%/96% for BHU-1 within 5 min, the photoreduction ratios of Cr(VI) were 97%, 95%, and 48% for BHU-1 within 30 min, and the photocatalytic decolorization ratios of RhB were 100% (within 60 min), 100% (within 90 min), and 31% (within 90 min) for BHU-1, respectively (Fig. 7d–g).[90]

4 Currently developed POM-based frameworks for photothermal catalysis

Photothermal catalysis based on photothermal conversion has gradually attracted great attention from researchers in the fields of energy and catalysis.[91–93] As a promising technology, it can dramatically enhance the catalytic activity and modulate the catalytic pathway due to a synergy between photochemical reaction pathways and thermochemical reaction pathways, thereby exhibiting excellent catalytic performance even under moderate conditions.[94] At present, photothermal catalysis can be mainly classified into three types: (1). photo-assisted thermal catalysis. The main reaction pathway is the thermal chemistry pathway, similar to traditional thermal catalysis.[95] (2). Thermal-assisted photocatalytic reaction. The main reaction mechanism is the photochemical pathway. (3). Photothermal co-catalysis. It integrated the thermochemical and photochemical pathways. The heat generated by the photothermal effect can promote the reaction process through the thermochemical pathway, and the light energy also contributes significantly to the apparent activity, resulting in a synergistic result of thermal and photochemical pathways that are different from the simple addition of these two pathways.[96] In the thermochemical pathway, the photothermal catalytic system can dissipate the absorbed photon energy into thermal energy under incident light irradiation, which can facilitate the transfer of charge carriers and enhance the catalytic activity. In the photochemical pathway, "hot" carriers (electrons or holes) can be generated upon light irradiation and then participated in the catalytic reactions.[97] Notably, it is often difficult to fully distinguish these two intertwined catalytic pathways during photothermal processes.[94,98] Thus, desir-

able photothermal catalysts for POMs should be constructed with the following design criteria: (i) accomplishing strong light absorption across the full solar spectrum, (ii) realizing high efficiency in photothermal conversion, and (iii) achieving excellent catalytic activity and stability.

For most POMs, the absorption is mainly in the UV-Vis region due to the ligand–metal charge-transfer (LMCT) transitions between O metals. The excited state energy generated after the transition is relatively high, mainly the photocatalytic reaction occurs, and there is almost no photothermal effect.[99] There are two common methods to achieve photothermal catalysis: the first is to disperse POMs into the organic framework structure with a wider and stronger absorption. The second is to combine organic ligands with POMs through ionic bonds, and then use the assembly method to form ordered assemblies or aggregates to achieve photothermal catalysis. Although the procedure is simple, the stability of assemblies and aggregates under photothermal conditions is an important issue. In addition, a class of reductive clusters, the transitions between metal ions at different valence states, and the d–d transitions and intervalence charge transfer (IVCT) caused by the connected oxygen bridge make POMs have longer wavelength absorption bands at long wavelengths. Considering the relatively low energy of NIR photons, it is difficult to directly activate the substrate molecules to participate in the reaction, while it can be effectively converted into heat energy by long-wavelength light irradiation (>700 nm), thus showing an obvious photothermal effect. This enables thermocatalytic conduction by photoirradiation in a POM-involved system. Compared with traditional thermal catalysis which uses external heating, photothermal catalysis uses *in situ* heating, which greatly reduces the heat loss in the catalysis. The generated heat is concentrated on the catalyst, creating a local heating effect and improving the catalytic efficiency. However, the stability of reduced clusters is an urgent problem, such as poor resistance to oxidation and dissociation.

To date, research on photothermal catalysis based on POMs is still in its infancy, and only a few literature studies are reported in the emerging area. A typical example is that inorganic clusters can serve as NIR photothermal centers. First, wheel-shaped giant POMs $\{Mo_{154}\}$ have a mixed-valent metal ion Mo^{5+}-O-Mo^{6+} structure at its equatorial position, resulting in strong NIR adsorption.[100] The combination of high photothermal conversion efficiency and catalytic performance effectively enables $\{Mo_{154}\}$ to perform cyclohexene oxidation under an O_2 atmosphere in water with the aid of phase transfer *via* cationic cyclodextrin (CDC) capped on giant clusters, as shown in Fig. 8a. The electrostatic interaction between CDC and POMs shortens the distance between the substrate and the catalyst, and the monodisperse structure of the complex ensures the effective collision probability between the substrate and the catalyst, thus improving the conversion of cyclohexene oxidation (Fig. 8b). The kinetic curve shows that the reaction rate under photothermal conditions is about 6 times faster than that under the traditional external heating conditions (Fig. 8c). The enhancement factor of photothermal catalysis is calculated to be in the range of 5 folds (Fig. 8d). In addition, large-sized substrates cannot enter the CDC cavity, enabling selective catalysis (Fig. 8e). Different from these known POM-based photothermal catalysts, these pioneering works for the first time realize the NIR photothermal catalytic integration of POMs and establish the photothermal catalytic system of POMs also demonstrating that photoinduced thermocatalysis is an effective strategy to enhance the conversion

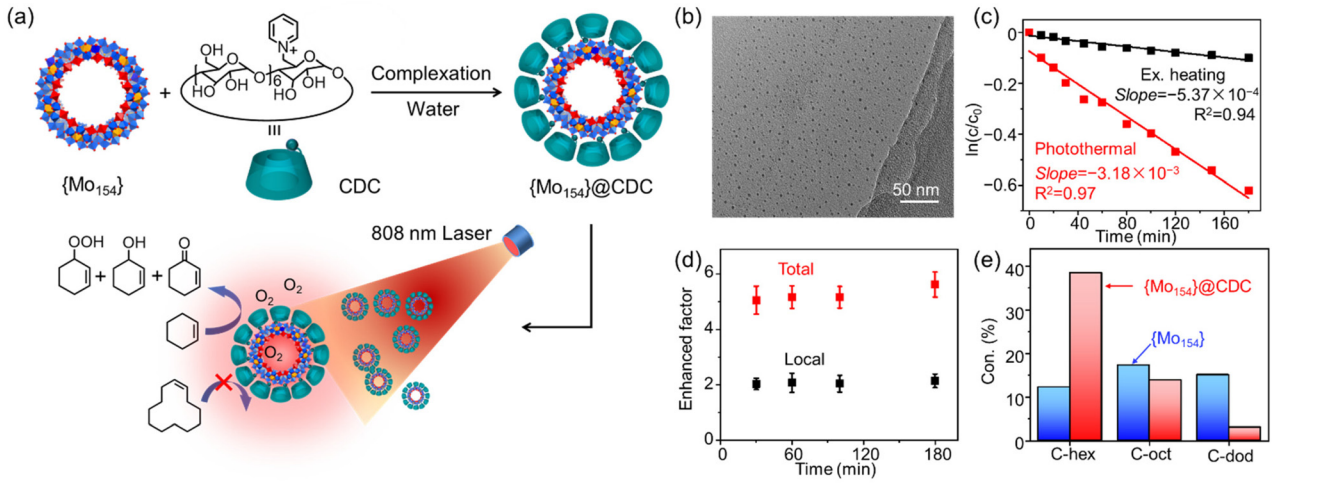

Fig. 8 (a) Schematic illustration for the complex comprising of $\{Mo_{154}\}$ and CDC, and its photothermal catalysis for the oxidation of olefins under irradiation with an 808 nm laser. (b) TEM image of $\{Mo_{154}\}$@CDC at 65 °C. (c) Catalytic kinetic curves of the substrate cyclohexene catalyzed by $\{Mo_{154}\}$@CDC *versus* the reaction time under different temperature conditions. (d) The calculated enhanced factors of Con.(P.T.)/Con.(R.T.) in the red square and Con.(P.T.)/Con.(Ex.H.) in the black square *versus* the reaction time. (e) Conversions of the oxidation of a series of alkenes (C-hex, cyclohexene; C-oct, cyclooctene; C-dod, and cyclododecene) over the catalyst $\{Mo_{154}\}$@CDC and the isolated $Na_{14}\{Mo_{154}\}$ cluster, Reproduced from ref. 100. Copyright 2021, AAAS.

and selectivity of the chemical reactions under mild conditions.

Other examples are organic linkers used as photosensitizers and photothermal components. Peng's group synthesized a PMo_{12}@Zr-Fc MOF nanosheet catalyst by decorating PMo_{12} with high Lewis acidity into Zr-Fc MOF nanosheets with excellent photothermal performance.[101] Owing to the abundance of accessible active sites and the low diffusion barrier of reactants, the obtained catalyst shows outstanding photothermal conversion ability and high catalytic activity in the solvent-free cycloaddition reaction with styrene oxide and CO_2 under simulated sunlight (Fig. 9a). This indicates that the incorporation of molecularly-dispersed PMo_{12} in Zr-Fc nanosheets significantly promotes the catalytic performance under mild conditions. 10.26 wt% PMo_{12}@Zr-Fc is used as the catalyst, the yield of cyclic carbonate is 86.77% and the turn-over number (TON) reaches 601. Due to the excellent photothermal properties of Zr-Fc MOF nanosheets, the PMo_{12}@Zr-Fc MOFs nanosheets also retain the same photothermal properties, and are utilized for solar-driven cycloaddition reactions without extra heating. When combined with the photothermal properties of the MOF matrix, functionalized MOFs with abundant Lewis acid sites and the tunability of PMo_{12} can enhance the high catalytic efficiency of heterogeneous catalysts, which provide a promising approach for designing solar-driven catalysts for CO_2 cycloaddition (Fig. 9b). Porphyrins also have good photocatalytic and photothermal conversion properties. A porphyrin Zr-MOF, PCN-222, with photothermal properties was prepared through the general procedure, followed by post-modification with stable POMs, $H_3PW_{12}O_{40}$, to obtain a novel porous POM@PCN-222.[102] The results indicate that it possesses an excelling photocatalytic activity in the efficient synthesis of pyridines with any additives, affording 1,4-dihydropyridine intermediates *in situ* from the *pseudo* four-component reaction between aldehydes, methyl acetoacetate, and ammonium acetate, followed by their photo-oxidation under visible LED illumination with O_2 as an oxidant. Compared to the pristine materials, the synergistic effect between MOFs and POMs realizes an increased catalytic performance. The strong interaction between PCN-222 and POMs prevent POMs leaching and the catalysts are highly active after three catalytic cycles. These examples are more in line with the type 2 mentioned earlier, in which photocatalysis plays a major role in reactions.

In the last year, Wu's group prepared polyethyleneimine (PEI)-covalently grafted the graphene oxide (GO), PEI-GO, as the NIR photothermal carrier center, and then electrostatically interacted with Co- and Ce-substituted Keggin-POMs, respectively, thereby preparing a three-in-one POM composite photothermal catalyst for NIR photothermal catalysis of the CO_2 cycloaddition reaction without solvents.[103] The introduction of the photothermal effect makes the prepared catalysts greatly enhance the CO_2 cycloaddition reaction under atmospheric pressure, while achieving the highest TOF value of the reaction so far. The catalyst can still maintain a relatively high catalytic activity and stability after 20 reuses. The photothermal catalysis mechanism shows that the transition metals in POMs act as Lewis acid sites to activate the epoxy substrate, PEI acts as the linker between GO and POMs to shorten the distance between the photothermal center and the catalytic center, and as a CO_2 adsorbent, it ensures the sufficient contact between the substrate and CO_2 and the ability to fully sense the temp-

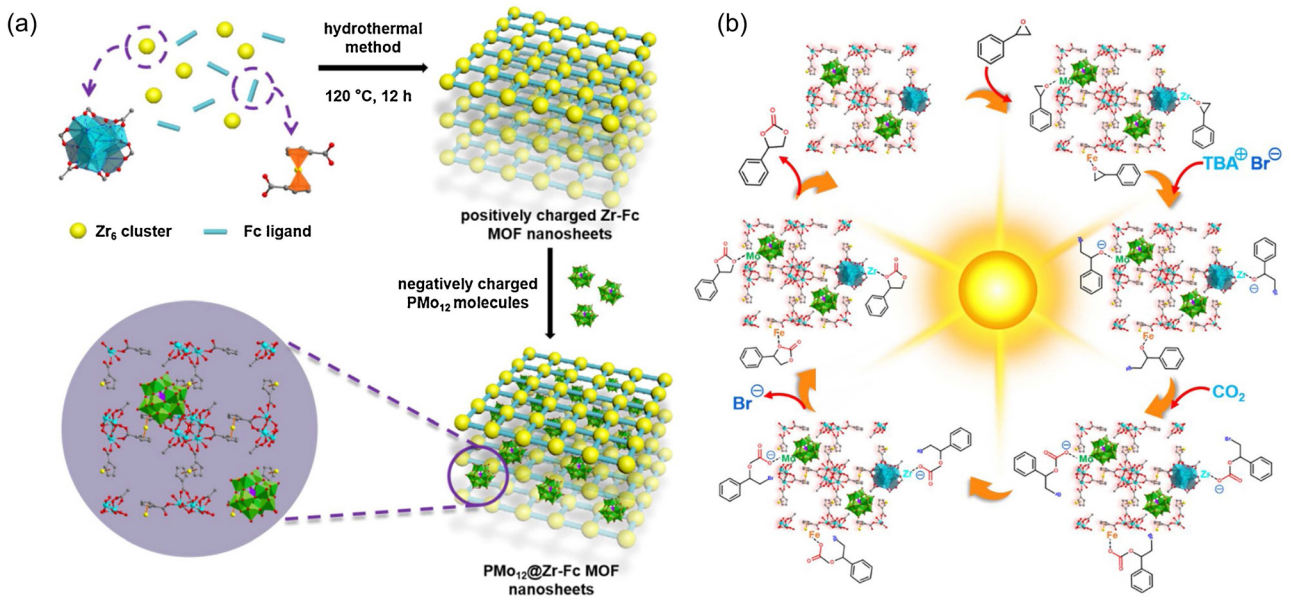

Fig. 9 (a) Synthesis process of PMo_{12}@Zr-Fc MOF nanosheets. The elements and clusters in the large version of the unit cell of PMo_{12}@Zr-Fc MOF nanosheets (with light purple background) are symbolized with following color: cyan, Zr; red, O; gray, C; yellow, Fe; violet tetrahedron, PO_4; green octahedron, MoO_6. Hydrogen atoms are omitted for clarity. (b) Mechanism of the cycloaddition of SO and CO_2 to form SC using the PMo_{12} decorated Zr-Fc MOF catalyst under sunlight. Reproduced with permission from ref. 101. Copyright 2021, Elsevier.

erature of the photothermal center, and finally synergistically realize an efficient conversion of CO_2 cycloaddition under ambient pressure. Moreover, they used 3,3′,5,5′-tetramethylbenzidine (TMB) as the precursor of the photothermal center, a stable charge transfer (TMB_{CT}) complex with a strong NIR photothermal effect was obtained by one-step oxidation and encapsulated with the catalysis components $Na_5PMo_{10}V_2O_{40}$, $Na_4PMo_{11}VO_{40}$, $K_4PW_{11}VO_{40}$, or $Na_3PMo_{12}O_{40}$ through the electrostatic interaction, resulting in complexes with enhanced photothermal properties.[104] Meanwhile, they exist in the form of 4–6 nm oligomers in an aqueous solution, and show high conversion and selectivity for the oxidation of toluene derivatives to alcohols under mild conditions. In the latest study, they constructed POM-modified AuNR composites by combining the high catalytic activity of PW_{12} and the NIR photothermal properties of Au nanorods through ligand replacement and electrostatic adsorption. The nanorod structure offer a unique plasmon-enhanced photothermal property and a lager specific surface area to load POMs. Under NIR irradiation, the observed kinetic constant of the selective oxidation of thioether derivatives is more than a 5-fold enhancement under external heating conditions. Moreover, the designed catalysts show excellent structural stability, catalytic stability, and photothermal conversion stability after 10 cycles.[105]

Photothermal catalysts with diverse POM-based framework structures and catalytic effects can be obtained, thereby realizing the catalysis of various substrates. However, there are still a few problems need to be solved. How to make full use of sunlight and achieve high photothermal conversion efficiency. Although the thermal effect plays a key role in the improvement of photothermal catalytic efficiency, *in situ* measurement of the temperature of the photothermal center remains an important but challenging problem. To develop more POM-based photothermal catalytic systems to further understand the mechanism of photothermal catalysis.

5 Summary and perspective

In this review, we have summarized the recent progress toward POM-based frameworks for photocatalysis and photothermal catalysis. Despite the remarkable advances achieved in this field, POM-based frameworks for photocatalysis and particularly photothermal catalysis are still in a very early developmental stage. Therefore, much effort should be devoted to their continued development, and some great challenges must be addressed. First, it is highly desired to develop cost-effective and stable POM-based framework photocatalysts and photothermal catalysts with higher activity. Considering the structure/composition tailorability, in addition to the synthesis of new stable framework structures, upon the introduction of long-wavelength-light-responsive units (*e.g.*, porphyrin units, up-conversion nanoparticles, plasmonic nanoparticles, *etc.*) into frameworks, light harvesting can be extended to NIR or full spectral regions; moreover, abundant catalytically active sites were embedded to achieve synergistically high catalytic activity or cascade catalysis. Second, more efforts should be devoted to achieving in-depth insights into the structure–activity relationship, which is of great significance to rationalize photocatalyst and photothermal design. In addition to the traditional characterization methods, Kelvin probe force microscopy-based spatially resolved surface photovoltage techniques have also been proven to be an effective means to unveil the photocatalytic mechanism. Last but not least, the integration of low-cost photothermal agents with highly active catalysis sites into POM-based framework catalysts is much preferred to achieve full spectral absorption, which would enable the reaction to proceed under moderate conditions. Given the great tunability of POM-based frameworks, we strongly believe that photocatalysis and photothermal catalysis over POM-based framework materials will possess a very bright future ahead.

Author contributions

X. Chen and L. Wu designed and outlined the draft of the review paper. H. Wu contributed to the scientific drawing of the manuscript. All authors contributed to the final polishing of the manuscript.

Conflicts of interest

There are no conflicts to declare.

Acknowledgements

This work was financially supported by the Natural Science Foundation of Henan Province, China (232300421369).

References

1 M. T. Pope and A. Müller, *Angew. Chem., Int. Ed. Engl.*, 1991, **30**, 34–48.
2 J.-X. Liu, X.-B. Zhang, Y.-L. Li, S.-L. Huang and G.-Y. Yang, *Coord. Chem. Rev.*, 2020, **414**, 213260.
3 J.-C. Liu, J.-W. Zhao, C. Streb and Y.-F. Song, *Coord. Chem. Rev.*, 2022, **471**, 214734.
4 S. S. Wang and G. Y. Yang, *Chem. Rev.*, 2015, **115**, 4893–4962.
5 K. Suzuki, N. Mizuno and K. Yamaguchi, *ACS Catal.*, 2018, **8**, 10809–10825.
6 J. Gu, W. Chen, G. G. Shan, G. Li, C. Sun, X. L. Wang and Z. Su, *Mater. Today Energy*, 2021, **21**, 100760.
7 Y. Liu, C. S. Tang, M. Cheng, M. Chen, S. Chen, L. Lei, Y. S. Chen, H. Yi, Y. K. Fu and L. Li, *ACS Catal.*, 2021, **11**, 13374–13396.
8 C. F. Li, K. Suzuki, N. Mizuno and K. Yamaguchi, *Chem. Commun.*, 2018, **54**, 7127–7130.

9 D. J. Zang and H. Q. Wang, *Polyoxometalates*, 2022, **1**, 9140006.
10 N. Li, J. Liu, B. X. Dong and Y. Q. Lan, *Angew. Chem., Int. Ed.*, 2020, **59**, 20779–20793.
11 P. T. Ma, F. Hu, J. P. Wang and J. Y. Niu, *Coord. Chem. Rev.*, 2019, **378**, 281–309.
12 N. I. Gumerova and A. Rompel, *Nat. Rev. Chem.*, 2018, **2**, 112.
13 R. Lamare, R. Ruppert, C. Boudon, L. Ruhlmann and J. Weiss, *Chem. – Eur. J.*, 2021, **27**, 16071–16081.
14 E. Raee, B. Q. Liu, Y. Q. Yang, T. Namani, Y. P. Cui, N. Sahai, X. P. Li and T. B. Liu, *Nano Lett.*, 2022, **22**, 4421–4428.
15 B. Gao, B. Li and L. X. Wu, *Chem. Commun.*, 2021, **57**, 10512–10515.
16 Y. Zhang, Y. F. Liu, D. Wang, J. C. Liu, J. W. Zhao and L. J. Chen, *Polyoxometalates*, 2023, 9140017, DOI: 10.26599/pom.2022.9140017.
17 H. Y. Zhang, W. L. Zhao, H. Q. Li, Q. H. Zhuang, Z. Q. Sun, D. Y. Cui, X. J. Chen, A. Guo, X. Ji, S. An, W. Chen and Y.-F. Song, *Polyoxometalates*, 2022, **1**, 9140011.
18 B. Li, W. Li, H. L. Li and L. X. Wu, *Acc. Chem. Res.*, 2017, **50**, 1391–1399.
19 Q. D. Liu, Q. H. Zhang, W. X. Shi, H. S. Hu, J. Zhuang and X. Wang, *Nat. Chem.*, 2022, **14**, 433–440.
20 S. Amthor, S. Knoll, M. Heiland, L. Zedler, C. Li, D. Nauroozi, W. Tobaschus, A. K. Mengele, M. Anjass, U. S. Schubert, B. Dietzek-Ivansic, S. Rau and C. Streb, *Nat. Chem.*, 2022, **14**, 321–327.
21 J. H. Kruse, M. Langer, I. Romanenko, I. Trentin, D. Hernández-Castillo, L. González, F. H. Schacher and C. Streb, *Adv. Funct. Mater.*, 2022, **32**, 2208428.
22 J. D. Xiao and H. L. Jiang, *Acc. Chem. Res.*, 2019, **52**, 356–366.
23 K. Y. Geng, T. He, R. Y. Liu, S. Dalapati, K. T. Tan, Z. P. Li, S. S. Tao, Y. F. Gong, Q. H. Jiang and D. L. Jiang, *Chem. Rev.*, 2020, **120**, 8814–8933.
24 J. Tian, H. Wang, D.-W. Zhang, Y. Liu and Z.-T. Li, *Natl. Sci. Rev.*, 2017, **4**, 426–436.
25 X. S. Zhang, S. H. Tong, D. L. Huang, Z. F. Liu, B. B. Shao, Q. H. Liang, T. Wu, Y. Pan, J. Huang, Y. Liu, M. Cheng and M. Chen, *Coord. Chem. Rev.*, 2021, **448**, 214177.
26 H. Wang, H. Wang, Z. W. Wang, L. Tang, G. M. Zeng, P. Xu, M. Chen, T. Xiong, C. Y. Zhou, X. Y. Li, D. L. Huang, Y. Zhu, Z. X. Wang and J. W. Tang, *Chem. Soc. Rev.*, 2020, **49**, 4135–4165.
27 X.-X. Li, D. Zhao and S.-T. Zheng, *Coord. Chem. Rev.*, 2019, **397**, 220–240.
28 A. Knebel and J. Caro, *Nat. Nanotechnol.*, 2022, **17**, 911–923.
29 Y. Li, M. Karimi, Y.-N. Gong, N. Dai, V. Safarifard and H.-L. Jiang, *Matter*, 2021, **4**, 2230–2265.
30 Q. Wang and D. Astruc, *Chem. Rev.*, 2020, **120**, 1438–1511.
31 M. Samaniyan, M. Mirzaei, R. Khajavian, H. Eshtiagh-Hosseini and C. Streb, *ACS Catal.*, 2019, **9**, 10174–10191.
32 C. T. Buru and O. K. Farha, *ACS Appl. Mater. Interfaces*, 2020, **12**, 5345–5360.
33 S. W. Zhang, F. X. Ou, S. G. Ning and P. Cheng, *Inorg. Chem. Front.*, 2021, **8**, 1865–1899.
34 Q. Fu, *ACS Appl. Mater. Interfaces*, 2023, **15**, 8275–8285.
35 F. L. Zhu, H. F. Bao, X. S. Wu, Y. L. Tao, C. Qin, Z. M. Su and Z. H. Kang, *ACS Appl. Mater. Interfaces*, 2019, **11**, 43206–43213.
36 P. Mialane, C. Mellot-Draznieks, P. Gairola, M. Duguet, Y. Benseghir, O. Oms and A. Dolbecq, *Chem. Soc. Rev.*, 2021, **50**, 6152–6220.
37 D.-Y. Du, J.-S. Qin, S.-L. Li, Z.-M. Su and Y.-Q. Lan, *Chem. Soc. Rev.*, 2014, **43**, 4615–4632.
38 X. J. Song, D. W. Hu, X. T. Yang, H. Zhang, W. X. Zhang, J. Y. Li, M. J. Jia and J. H. Yu, *ACS Sustainable Chem. Eng.*, 2019, **7**, 3624–3631.
39 S. Wang, Y. W. Liu, Z. Zhang, X. H. Li, H. R. Tian, T. T. Yan, X. Zhang, S. M. Liu, X. W. Sun, L. Xu, F. Luo and S. X. Liu, *ACS Appl. Mater. Interfaces*, 2019, **11**, 12786–12796.
40 Q. Huang, J. Liu, L. Feng, Q. Wang, W. Guan, L. Z. Dong, L. Zhang, L. K. Yan, Y. Q. Lan and H. C. Zhou, *Natl. Sci. Rev.*, 2020, **7**, 53–63.
41 H. N. Miras, L. Vila-Nadal and L. Cronin, *Chem. Soc. Rev.*, 2014, **43**, 5679–5699.
42 Y. W. Liu, S. M. Liu, D. F. He, N. Li, Y. J. Ji, Z. P. Zheng, F. Luo, S. X. Liu, Z. Shi and C. W. Hu, *J. Am. Chem. Soc.*, 2015, **137**, 12697–12703.
43 X. X. Li, C. C. Deng, D. Zhao, H. Yu, Q. X. Zeng and S. T. Zheng, *Dalton Trans.*, 2018, **47**, 16408–16412.
44 D. G. Ke, S. L. Huang and G.-Y. Yang, *Inorg. Chem.*, 2022, **61**, 20080–20086.
45 Y. Zhou, G. Zhang, B. Li and L. Wu, *ACS Appl. Mater. Interfaces*, 2020, **12**, 30761–30769.
46 A. Macdonell, N. A. Johnson, A. J. Surman and L. Cronin, *J. Am. Chem. Soc.*, 2015, **137**, 5662–5665.
47 G. H. Zhang, X. Y. Li, G. Chen, Y. Zhang, M. F. Wei, X. F. Chen, B. Li, Y. Q. Wu and L. X. Wu, *Nat. Commun.*, 2023, **14**, 975.
48 T. Chang, D. Qu, B. Li and L. X. Wu, *Molecules*, 2022, **27**, 7447.
49 P. F. Wu, Y. Wang, B. Huang and Z. C. Xiao, *Nanoscale*, 2021, **13**, 7119–7133.
50 W. M. Guan, B. Li and L. X. Wu, *Dalton Trans.*, 2022, **51**, 4541–4548.
51 W. T. Xu, X. K. Pei, C. S. Diercks, H. Lyu, Z. Ji and O. M. Yaghi, *J. Am. Chem. Soc.*, 2019, **141**, 17522–17526.
52 R. Ma, N. F. Liu, T.-T. Lin, T. B. Zhao, S.-L. Huang and G.-Y. Yang, *J. Mater. Chem. A*, 2020, **8**, 8548–8553.
53 X. Q. Yu, C. Y. Li, Y. C. Ma, D. H. Li, H. Li, X. Y. Guan, Y. S. Yan, V. Valtchev, S. L. Qiu and Q. R. Fang, *Microporous Mesoporous Mater.*, 2020, **299**, 110105.
54 Y. Zhao, Z. F. Wang, J. Gao, Z. F. Zhao, X. Li, T. Wang, P. Cheng, S. Q. Ma, Y. Chen and Z. J. Zhang, *Nanoscale*, 2020, **12**, 21218–21224.
55 Y. R. Zhang, D. H. Yang, S. L. Qiao and B. H. Han, *Langmuir*, 2021, **37**, 10330–10339.

56 H. Li, J. L. Liu, M. D. Wang, X. M. Ren, C. Z. Li, Y. Q. Ren and Q. H. Yang, *Sol. RRL*, 2020, **5**, 2000641.
57 J. M. Wang, X. Xu, L. M. Zhao and B. Yan, *J. Mater. Chem. C*, 2021, **9**, 9492–9498.
58 W. X. Wang, Y. T. Song, J. Y. Chen, Y. Y. Yang, J. W. Wang, Y. Song, J. T. Ni, M. L. Tang, J. G. Zhao, Y. Sun, T. D. Sun and J. S. Peng, *J. Mater. Chem. B*, 2022, **10**, 1128–1135.
59 S. B. Yu, F. R. Lin, J. Tian, J. L. Yu, D. W. Zhang and Z. T. Li, *Chem. Soc. Rev.*, 2022, **51**, 434–449.
60 W. Q. Xu, J. Y. Chao, B. H. Tang, Z. T. Li, J. F. Xu and X. Zhang, *Chem. – Eur. J.*, 2022, **28**, e202202200.
61 F. X. Duan, X. T. Liu, D. Qu, B. Li and L. X. Wu, *CCS Chem.*, 2020, **2**, 2676–2687.
62 T. Iwano, S. Miyazawa, R. Osuga, J. N. Kondo, K. Honjo, T. Kitao, T. Uemura and S. Uchida, *Commun. Chem.*, 2019, **2**, 9.
63 B. Li and L. X. Wu, *Polyoxometalates*, 2023, **2**, 9140016.
64 J. Tian, Z. Y. Xu, D. W. Zhang, H. Wang, S. H. Xie, D. W. Xu, Y. H. Ren, H. Wang, Y. Liu and Z. T. Li, *Nat. Commun.*, 2016, **7**, 11580.
65 L. Yue, S. Wang, D. Zhou, H. Zhang, B. Li and L. X. Wu, *Nat. Commun.*, 2016, **7**, 10742.
66 S. Zhang, B. Qin, J.-F. Xu and X. Zhang, *ACS Mater. Lett.*, 2021, **3**, 331–336.
67 P. Sun, Y. Q. Li, B. Qin, J.-F. Xu and X. Zhang, *ACS Mater. Lett.*, 2021, **3**, 1003–1009.
68 F. R. Jiang, B. Li and L. X. Wu, *Inorg. Chem.*, 2022, **61**, 20587–20595.
69 W. M. Guan, G. X. Wang, J. B. Ding, B. Li and L. X. Wu, *Chem. Commun.*, 2019, **55**, 10788–10791.
70 G. H. Zhang, B. Li, Y. Zhou, X. F. Chen, B. Li, Z. Y. Lu and L. X. Wu, *Nat. Commun.*, 2020, **11**, 425.
71 Y. N. Bo, C. Gao and Y. J. Xiong, *Nanoscale*, 2020, **12**, 12196–12209.
72 A. Solé-Daura, Y. Benseghir, M.-H. Ha-Thi, M. Fontecave, P. Mialane, A. Dolbecq and C. Mellot-Draznieks, *ACS Catal.*, 2022, **12**, 9244–9255.
73 S.-M. Liu, Z. Zhang, X. H. Li, H. J. Jia, M. W. Ren and S. X. Liu, *Adv. Mater. Interfaces*, 2018, **5**, 1801062.
74 M. Lu, M. Zhang, J. Liu, T. Y. Yu, J. N. Chang, L. J. Shang, S. L. Li and Y. Q. Lan, *J. Am. Chem. Soc.*, 2022, **144**, 1861–1871.
75 C. B. Bie, L. X. Wang and J. G. Yu, *Chem*, 2022, **8**, 1567–1574.
76 A. Kudo and Y. Miseki, *Chem. Soc. Rev.*, 2009, **38**, 253–278.
77 K. Takanabe, *ACS Catal.*, 2017, **7**, 8006–8022.
78 Y. C. Zhang, N. Afzal, L. Pan, X. Zhang and J. J. Zou, *Adv. Sci.*, 2019, **6**, 1900053.
79 P. Zhang, J. Zhang and J. Gong, *Chem. Soc. Rev.*, 2014, **43**, 4395–4422.
80 G. Paille, M. Gomez-Mingot, C. Roch-Marchal, B. Lassalle-Kaiser, P. Mialane, M. Fontecave, C. Mellot-Draznieks and A. Dolbecq, *J. Am. Chem. Soc.*, 2018, **140**, 3613–3618.
81 G. Paille, M. Gomez-Mingot, C. Roch-Marchal, M. Haouas, Y. Benseghir, T. Pino, M. H. Ha-Thi, G. Landrot, P. Mialane, M. Fontecave, A. Dolbecq and C. Mellot-Draznieks, *ACS Appl. Mater. Interfaces*, 2019, **11**, 47837–47845.
82 L. Jiao, Y. Y. Dong, X. Xin, L. Qin and H. J. Lv, *Appl. Catal., B*, 2021, **291**, 120091.
83 K. Maru, S. Kalla and R. Jangir, *Dalton Trans.*, 2022, **51**, 11952–11986.
84 J. C. He, Q. X. Han, J. Li, Z. L. Shi, X. Y. Shi and J. Y. Niu, *J. Catal.*, 2019, **376**, 161–167.
85 J. C. Jiao, X. M. Yan, S. Z. Xing, T. Zhang and Q. X. Han, *Inorg. Chem.*, 2022, **61**, 2421–2427.
86 J. C. Jiao, H. Sun, C. Si, J. B. Xu, T. Zhang and Q. X. Han, *ACS Appl. Mater. Interfaces*, 2022, **14**, 16386–16393.
87 Y. N. Liu, J. Wang, K. H. Ji, S. Meng, Y. H. Luo, H. F. Li, P. T. Ma, J. Y. Niu and J. P. Wang, *J. Catal.*, 2022, **416**, 149–156.
88 Y. S. Li, M. X. Liu and L. Chen, *J. Mater. Chem. A*, 2017, **5**, 13757–13762.
89 C.-C. Wang, J.-R. Li, X.-L. Lv, Y.-Q. Zhang and G. S. Guo, *Energy Environ. Sci.*, 2014, **7**, 2831–2867.
90 L. Yang, Z. Zhang, C. N. Zhang, S. Li, G. C. Liu and X. L. Wang, *Inorg. Chem. Front.*, 2022, **9**, 4824–4833.
91 D. Mateo, J. L. Cerrillo, S. Durini and J. Gascon, *Chem. Soc. Rev.*, 2021, **50**, 2173–2210.
92 M. Ghoussoub, M. Xia, P. N. Duchesne, D. Segal and G. Ozin, *Energy Environ. Sci.*, 2019, **12**, 1122–1142.
93 L. L. Zhu, M. M. Gao, C. K. N. Peh and G. W. Ho, *Mater. Horiz.*, 2018, **5**, 323–343.
94 C. Q. Song, Z. H. Wang, Z. Yin, D. Q. Xiao and D. Ma, *Chem Catal.*, 2022, **2**, 52–83.
95 H. B. Zhang, T. Wang, J. J. Wang, H. M. Liu, T. D. Dao, M. Li, G. G. Liu, X. G. Meng, K. Chang, L. Shi, T. Nagao and J. H. Ye, *Adv. Mater.*, 2016, **28**, 3703–3710.
96 C. Q. Song, X. Liu, M. Xu, D. Masi, Y. G. Wang, Y. C. Deng, M. T. Zhang, X. T. Qin, K. Feng, J. Yan, J. Leng, Z. H. Wang, Y. Xu, B. H. Yan, S. Y. Jin, D. S. Xu, Z. Yin, D. Q. Xiao and D. Ma, *ACS Catal.*, 2020, **10**, 10364–10374.
97 Z. J. Wang, H. Song, H. M. Liu and J. H. Ye, *Angew. Chem., Int. Ed.*, 2020, **59**, 8016–8035.
98 G. X. Wang, B. Li and L. X. Wu, *J. Mater. Chem. A*, 2022, **10**, 21884–21892.
99 X. P. Kong, G. F. Wan, B. Li and L. X. Wu, *J. Mater. Chem. B*, 2020, **8**, 8189–8206.
100 X. F. Chen, G. H. Zhang, B. Li and L. X. Wu, *Sci. Adv.*, 2021, **7**, eabf8413.
101 Z. Fang, Z. Deng, X. Y. Wan, Z. Y. Li, X. Ma, S. Hussain, Z. Z. Ye and X. S. Peng, *Appl. Catal., B*, 2021, **296**, 120329.
102 S. Karamzadeh, E. Sanchooli, A. R. Oveisi, S. Daliran and R. Luque, *Appl. Catal., B*, 2022, **303**, 120815.
103 X. F. Chen, M. F. Wei, A. B. Yang, F. R. Jiang, B. Li, O. A. Kholdeeva and L. X. Wu, *ACS Appl. Mater. Interfaces*, 2022, **14**, 5194–5202.
104 X. F. Chen, A. B. Yang, G. X. Wang, M. F. Wei, N. Liu, B. Li and L. X. Wu, *Chem. Eng. J.*, 2022, **446**, 137134.
105 G. X. Wang, X. F. Chen, B. Li and L. X. Wu, *Inorg. Chem. Front.*, 2023, **10**, 1852–1862.